THE JOURNAL OF BIOLOGICAL CHEMISTRY VOL. 285, NO. 53, pp. 41874–41885, December 31, 2010

Identification of the NC1 Domain of α3 Chain as Critical for α3α4α5 Type IV Collagen Network Assembly[S]

Received for publication, May 30, 2010, and in revised form, August 8, 2010 Published, JBC Papers in Press, September 16, 2010, DOI 10.1074/jbc.M110.149534

Valerie LeBleu[‡§], Malin Sund[‡], Hikaru Sugimoto[‡], Gabriel Birrane[¶], Keizo Kanasaki[‡], Elizabeth Finan[‡], Caroline A. Miller[‖], Vincent H. Gattone II[‖], Heather McLaughlin[‡], Charles F. Shield III[**], and Raghu Kalluri[‡§‡‡1]

From the [‡]Division of Matrix Biology and the [¶]Division of Experimental Medicine, Beth Israel Deaconess Medical Center and Harvard Medical School and the [§]Department of Biological Chemistry and Molecular Pharmacology, Harvard Medical School, Boston, Massachusetts 02115, the [‖]Department of Anatomy and Cell Biology, Indiana University School of Medicine, Indianapolis, Indiana 46227, the [**]Department of Surgery, University of Kansas School of Medicine, Wichita, Kansas 66160, and [‡‡]Harvard-MIT Division of Health Sciences and Technology, Boston, Massachusetts 02139

The network organization of type IV collagen consisting of α3, α4, and α5 chains in the glomerular basement membrane (GBM) is speculated to involve interactions of the triple helical and NC1 domain of individual α-chains, but *in vivo* evidence is lacking. To specifically address the contribution of the NC1 domain in the GBM collagen network organization, we generated a mouse with specific loss of α3NC1 domain while keeping the triple helical α3 chain intact by connecting it to the human α5NC1 domain. The absence of α3NC1 domain leads to the complete loss of the α4 chain. The α3 collagenous domain is incapable of incorporating the α5 chain, resulting in the impaired organization of the α3α4α5 chain-containing network. Although the α5 chain can assemble with the α1, α2, and α6 chains, such assembly is incapable of functionally replacing the α3α4α5 protomer. This novel approach to explore the assembly type IV collagen *in vivo* offers novel insights in the specific role of the NC1 domain in the assembly and function of GBM during health and disease.

Type IV collagen genes encode six distinct α-chains, α1 to α6 chains, which are expressed in development and tissue-specific patterns to allow for distinct type IV collagen composition in basement membranes (1–4). The distinct supramolecular organization of type IV collagen networks likely provides a unique structural stability and distinct biochemical properties to the basement membranes they compose. Although genetically distinct, all chains of type IV collagen are highly homologous and assemble to form an irregular polyglonal scaffold that interacts with other extracellular proteins (2). The unique primary and secondary structure of type IV collagen chains likely allow for their intrinsic ability to assemble into specific networks. Each chain is composed of an N-terminal or 7S domain and a C-terminal or non-collagenous (NC1) domain composed of ~230 amino acids, separated by a major collagenous domain of ~1400 amino acid residues composed of Gly-*X*-Y repeats, in which *X* is proline or lysine, and *Y* is hydroxyproline or hydroxylysine. In theory, six chains of type IV collagen could assemble into 56 possible protomers combinations, yet in mammals only three protomers, α1α2α1, α3α4α5, and α5α6α5, have been speculated using *in vitro* assays (5, 6).

The highest degree of sequence divergence between chains is observed in the NC1 domain, and *in vitro* studies suggest a role for the NC1 domain as the recognition and nucleation center for the folding of three chains of type IV collagen into protomers (7–13). *In vitro* self-assembly studies of type IV collagen NC1 domains (7, 12, 14), kinetics (15, 16) and crystal structure analyses (15, 17), and rotary shadowing microscopy of heat-denatured chains (18) suggest that the NC1 domain offers recognition sequences for chain selection (16). Immunoprecipitation studies on purified type IV collagen hexamers extracted mainly from bovine tissues indicate a strict chain composition of type IV collagen networks (14, 16, 19). At the protomer level, *in vitro* studies suggest a role for the NC1 domain in chain selection; that is, assembly of the purified α1 and α2 NC1 domains into α1α2α1 NC1 trimers and differential affinity of α2 NC1 domain as a mechanism for chain discrimination in α1α2α1 NC1 trimers *in vitro* assembly (15). Mutant NC1 domains of the type IV collagen α5 chain also identify NC1 sites for the *in vitro* assembly of recombinant NC1 monomers into α3α4α5 NC1 trimers (20). These studies, however, resort to *in vitro* self-assembly analyses using extracted and highly processed type IV collagen NC1 domains or expression of mutant proteins in cell culture, which might incorrectly recapitulate assembly dynamics of full-length chains *in vivo*. The underlying mechanism for α3α4α5 protomer assembly and network formation remains unknown, and it remains unclear whether the NC1 domain plays a definite role in protomer chain selection *in vivo*.

Protomer assembly is a regulated cellular process, likely guided by chaperone proteins in the Golgi apparatus. Once assembled, the protomers are then secreted in the extracellular space and self-assemble in complex networks (2, 21). After intracellular protomer assembly, self-assembly of type IV collagen in the extracellular space is also under selective control. The α2α1α1/α2α1α1, α4α3α5/α4α5α3, and α2α1α1/α6α5α5 networks are found in specialized basement membranes within the kidney glomerulus (13). The selective mechanism for protomer assembly into type IV collagen network is unknown. Indeed, mutations in the collagenous domain can also lead the

[S] The on-line version of this article (available at http://www.jbc.org) contains supplemental Figs. 1 and 2.

[1] To whom correspondence should be addressed: Harvard Medical School, Beth Israel Deaconess Medical Center, Division of Matrix Biology, Center for Life Sciences E/CLS 11-090, 330 Brookline Ave., Boston, MA 02215. Tel.: 617-735-4601; Fax: 617-735-4602; E-mail: rkalluri@bidmc.harvard.edu.

loss of α3α4α5 protomer, perhaps by diminishing the stability of the protomer after assembly (22–24).

Despite insights gained from *in vitro* studies and genetic knock-out mouse model studies, the mechanism for chain selection in protomer network assembly and the role of the NC1 domain in these processes remain to be determined. To gain insights on the mechanism of type IV collagen assembly *in vivo* in the GBM,[2] we engineered a mouse in which the mouse α3NC1 domain was replaced with the human α5NC1 domain, keeping the 7 S- and collagenous domains of α3 chain intact. This NC1 domain genetic swapping strategy allows for the biological and biochemical analyses of type IV collagen in network assembly.

EXPERIMENTAL PROCEDURES

Cloning of the Mouse α3NC1 Knock-out/Human α5NC1 Knock-in Targeting Vector—This construct was generated with the aim of removing the NC1 domain from the mouse type IV collagen α3 chain and replacing it with the NC1 domain of the human type IV collagen α5 chain. A BAC clone (404A6, Invitrogen) containing the end of the mouse α3 type IV collagen gene was used to generate the long (4.5 kb) and short (2.1 kb) arms of the construct by PCR. The primers 5′-CAG TGC GGC CGC ATA ATT CTC CCA AAA TAC TTC-3′ and 5′-GAA GCC GCG GAT TCT TGT ACC AGT GGC CGG CG-3′ (long arm) and 5′-TCT TAG GTA CCA AAG TCA TGA CTT AGA ACA TG-3′ and 5′-TGT GCG AAT TCA GTG GAG AAC ATG AGA GGA TGA TG-3′ (short arm) were used for the PCR of the long and short arms, respectively. Novel NotI and SacII as well as KpnI and EcoRI restriction sites were included in the primers, thus, generating restriction sites used during subsequent subcloning. The human α5 NC1 domain (1.8 kb) was sequenced from a human kidney cDNA library (Stratagene) using the primers 5′-CTG TTG CAC CGC GGT TTC TTA TTA CAC GCC ACA GCC-3′ and 5′-ATC CTA GGA ACA TAT ATC TTT AAT TAA ATT TAT ATT G-3′. The primers contain novel SacII and BamHI restriction sites used for further subcloning purposes. All fragments were subcloned using the TOPO TA Cloning System (Invitrogen) and sequenced to ensure the correct amplification. The SacII restriction site in the 4.5-kb genomic fragment from the mouse α3 gene and in the human α5 cDNA fragment makes it possible to join the mouse and human sequences and maintain the correct reading frame. At the junction site there is a change from a methionine-arginine-aspartic acid amino acid sequence to an isoleucine-arginine-glycine sequence before the start of the actual NC1 domain. The human α5 cDNA fragment contains an translation termination site and the polyadenylation sequence for the hybrid mouse α3NC1/human α5NC1 chain. To ensure no transcription beyond the cDNA fragment, which would lead to the addition of mouse α3 sequences 3′ of the hybrid chain, we added transcription termination signals in all three reading frames at the end of the human α5 cDNA fragment. The two genomic fragments as well as the human α5 cDNA fragment were subsequently cloned into the Triple LoxP vector generating the final construct used for gene targeting (Fig. 1*A*). After targeting the COL4A3 gene, the NC1 domain of the mouse α3 gene was replaced by the novel hybrid allele. The Triple LoxP vector contains *Neo* and TK cassettes used as selection marker during gene targeting.

Generation and Genotyping of the Mouse a3NC1 Knock-out/Human a5NC1 Knock-in Mice ($A3_mA5_h$)—The targeting vector was linearized, purified, and electroporated into embryonic stem cells at the Brigham and Women's Hospital transgenic facility, Boston, MA. G418-resistant embryonic stem cells clones were screened by Southern blot analysis using a 5′ external probe. This probe was generated by PCR from the 404A6 BAC using the primers 5′-GGG AGC ACC AGG TAC CCC CGG TCT TCC CGG3-′ and 5′-TAC AGT AAG GGT ACC CTT AGT GAT GCA GGG CTG-3′ and subcloned into the Topo vector. A correctly targeted clone will be identified by a 2.1-kb band as compared with the 4.4-kb wild-type allele. 175 colonies were screened, and 3 correctly targeted colonies were identified. Two clones were injected into blastocysts and implanted into pseudopregnant mice, and the resulting founders were bred to C57BL/6J mice to generate inbred mutant strains. Mice were subsequently genotyped by PCR using the forward primer 5′-GTC TGG ATG GAT TGC CAG GCT-3′ and reverse primer 5′-CAT CGG CTA ATT GCT GTC CTC-3′, which amplify a 600-bp fragment from the mutant allele (knock-in (KI)) containing both mouse α3 and human α5 sequence. The wild-type (WT) 300-bp fragments was amplified using forward primer 5′-CAG CTG CCT GCA GCG ATT CAC-3′ and reverse primer 5′-GGG ACA CGG AGG GAT ACA GTA-3′. PCR reactions were carried out under the following conditions: 35 times (95 °C for 1 min, 60 °C for 1 min, 72 °C for 1 min).

Animal Care—The generation and characterization of the renal disease progression in A3KO mice were previously described (25). The mice were backcrossed (10+ generations) from 129Sv to C57BL/6J genetic background. $A3_mA5_h$ founder mice were back-crossed to C57BL/6J wild-type mice purchased from Charles River. The resultant F1 progeny with germ line transmission of the $A3_mA5_h$ KI allele were derived from a single line of founder and mated with C57BL/6J wild-type mice and $A3_mA5_h$ heterozygote to obtain $A3_mA5_h$ KI mice. All mice in this study were housed under standard conditions at the Beth Israel Deaconess Medical Center animal facility. All animal studies were reviewed and approved by the Animal Care and Use Committee of the Beth Israel Deaconess Medical Center.

Human Sample—Normal human kidney tissue was obtained from rejected kidney grafts and was provided by Dr. C. Shield III under appropriate patient consent and institutional approval.

RT-PCR and in Situ Hybridization—RNA from kidneys of wild-type and $A3_mA5_h$ KI mice was extracted using TRIzol according to the manufacturer's instructions. After DNase I treatment, cDNA was synthesized using High Capacity cDNA Reverse Transcription kit from AB Biosystems. Forward primer 5′-GGT TCA GAA CTG GCA CCC GAG-3′ and reverse primer 5′-CCC GGT GAC CAT GTT CTT AGG C-3′ were used to amplify the human specific α5 NC1 200pb PCR product, and forward primer 5′-CGT GGG CCG CCC TAG GCA CCA-3′ and reverse primer 5′-TTG GCC TTA GGG TTC

[2] The abbreviations used are: GBM, glomerular basement membrane; KI, knock-in; ECM, extracellular matrix; IP, immunoprecipitation.

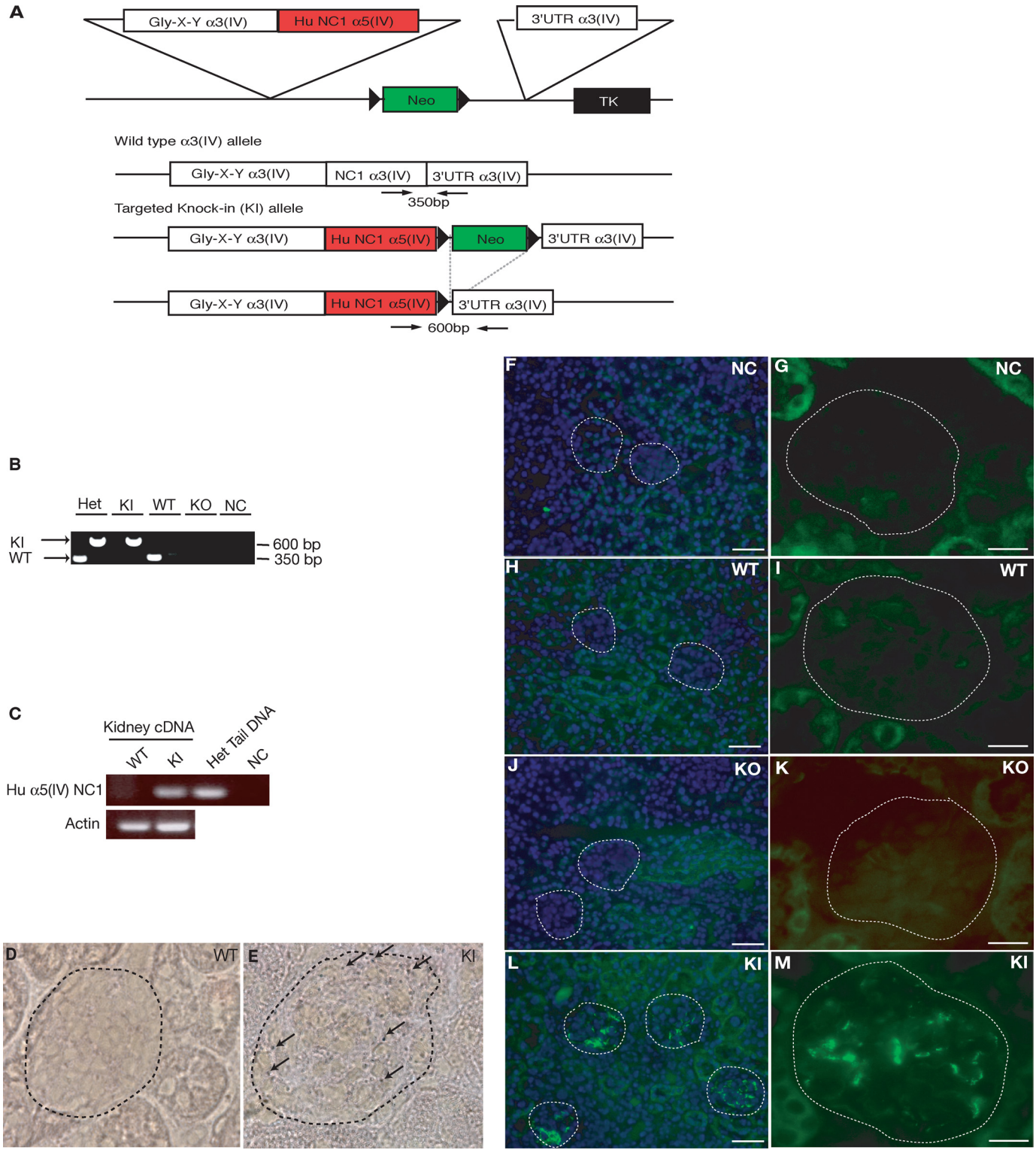

FIGURE 1. **Generation of the $A3_mA5_h$ KI mice.** *A*, construction of gene targeting vector and validation of target insertion is shown. A 4.5-kb fragment for mouse α3 Gly-*X*-Y collagenous domain was inserted adjunct to a 1.8-kb fragment for human α5NC1 domain before the *Neo* cassette. A 2.1-kb fragment for mouse α3 3′-UTR was inserted after the *Neo* cassette. *Arrows* indicate genotyping primers. *TK*, thymidine kinase. *B*, genotyping results from PCR from tail genomic DNA, with a 600-bp PCR product for KI allele and 350-bp PCR product for the wild-type α3 allele. *Het*, heterozygous. *C*, primers were designed to amplify a fragment from the cDNA sequence of human α5NC1 domain. No amplification in the WT kidney cDNA (negative control) indicates primer specificity. The 200-bp-expected PCR product was detected in $A3_mA5_h$ heterozygote tail genomic DNA containing human α5NC1 cDNA sequence (positive control) and in $A3_mA5_h$ KI kidney cDNA, indicating human α5NC1 expression in the $A3_mA5_h$ KI mouse. Actin amplification was used for internal control. *D–E*, *in situ* hybridization is shown using DIG-labeled human α5NC1-specific probe revealed glomeruli expression in $A3_mA5_h$ KI kidney section (*E*) but no expression in control WT kidney section (*D*). Glomeruli are *circled*; *arrows* point to human α5NC1 expression. *F–M*, shown is immunolabeling of kidney tissue sections using anti-human α5NC1 antibody, which reveals positive glomeruli labeling in the KI kidney (*L–M*) but not in the KO (*J–K*) and WT (*H–I*) control or secondary antibody negative control (*NC*) only (*F–G*). Glomeruli are *circled*. Magnification: *left panel*, ×200; the *scale bar* indicates 50 μm; *right panel*, ×630, the *scale bar* indicates 10 μm.

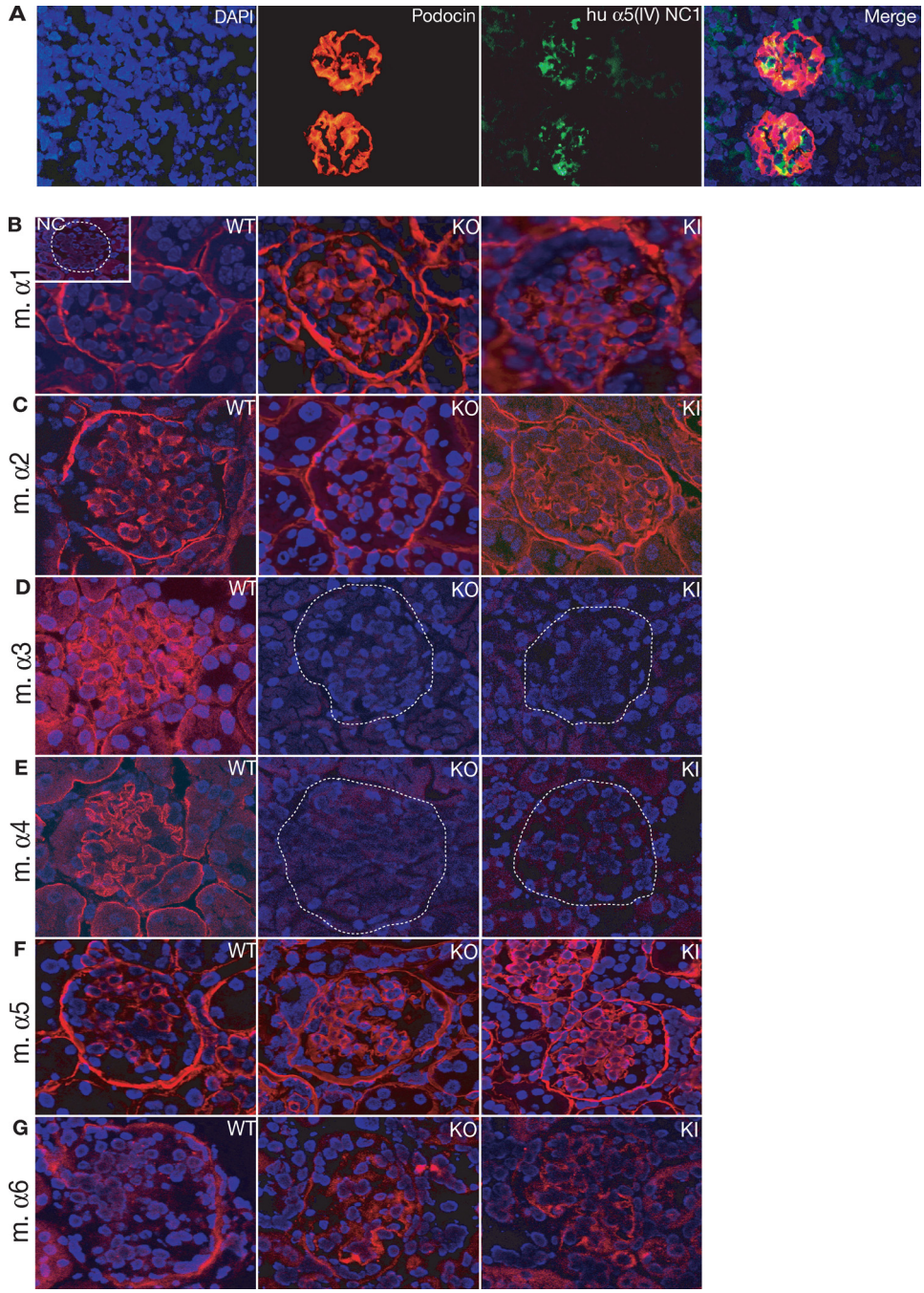

FIGURE 2. **Mouse kidney type IV collagen immunolabeling.** *A*, immunolabeling of KI kidney frozen section for podocin (*red*) and human (*hu*) α5NC1 (*green*) is shown. DAPI nuclear labeling is in *blue*. Magnification: ×400. *B–G*, shown is immunolabeling of WT, KO, and KI frozen sections for α1NC1 (*B*), α2NC1 (*C*), α3NC1 (*D*), α4NC1 (*E*), α5NC1 (*F*) and α6NC1 (*G*). Magnification, ×630. *NC*, negative control, secondary antibody only. Glomeruli are circled in *panels D* and *E*.

AGG GGG G-3′ were used to amplify the 250-bp mouse β-actin PCR product, 45× (95 °C for 30 s, 60 °C for 30 s, 72 °C for 30 s). These primers were used as probe for *in situ* hybridization. The probes were labeled using the Digoxigenin oligonucleotide 3′-end labeling kit, second generation (Roche Applied Science). Kidney frozen sections (15 μm) on 3-aminopropyltriethoxysilane-coated slides were fixed with 4% paraformaldehyde in PBS for 15 min. The slides were then washed and treated with 0.2 N HCl for 15 min at room temperature and incubated with prewarmed proteinase K (20 μg/ml) for 15 min. The sections were then fixed in 4% paraformaldehyde in PBS, washed, pre-hybridized with hybridization buffer (50% formamide, 2× SSC, 50 mM phosphate buffer, pH 7.0, 1× Denhardt's, 5% dextran) and subsequently hybridized with Digoxigenin labeled probe in 1 μg/ml hybridization buffer overnight in 37 °C. The slides were then washed in wash buffer (100 mM Tris HCl, pH 7.5, 150 mM NaCl) for 10 min followed by 30-min incubations with 1× blocking buffer (Roche Applied Science) and incubated with 1:5000 diluted anti-Digoxigenin antibody (Roche Applied Science) for 30 min, washed in wash buffer twice for 15 min, and equilibrated with detection buffer (100 mM Tris-HCl, pH 9.5, 100 mM NaCl) for 3 min. The sections were then incubated with color substrate (Roche Applied Science) in detection buffer, and Tris-EDTA buffer was used to stop the reaction.

Light Microscopy Staining and Morphometric Analyses—Kidneys were harvested and fixed in formalin. The tissues were then embedded in paraffin, and paraffin sections were used for periodic acid-Schiff and Masson-Trichrome staining under standard conditions (Histology Core Facility, Beth Israel Deaconess Medical Center). Morphometric analyses for the histological assessment of renal injury, glomerular sclerosis, tubular atrophy, and interstitial fibrosis, were performed as previously described (26, 27).

Immunohistochemistry—Sagittal sections of kidney were embedded in Optimal Cutting Temperature compound and snap-frozen in liquid nitrogen. A mouse-on-mouse (Vector Laboratory) immunodetection kit was used to immunolabel 4–10-μm frozen kidney sections with the monoclonal antibody against human α5 NC1 domain (dilution 1:200, Wieslab AB) following the instructions provided by the kit's manufacturer, omitting the avidin/biotin blocking step. These slides were mounted with Vectashield Mounting Media with DAPI (Vector Laboratory) and glass coverslips. Kidney sections were immunolabeled using standard immunostaining methods for the detection of podocin (generated by Dr. Peter Mundel, University of Miami, FL) and α1-α6NC1 domains. Briefly, frozen kidney sections (5 μm) were fixed in 0.2 N HCl 20 min at room

temperature. Slides were then washed twice with phosphate-buffered saline (PBS) and blocked in 2% bovine albumin serum (BSA) in PBS for 1 h at room temperature. The slides were incubated with primary antibody against type IV collagen chains (dilution 1:200, a gift from Dr. Cosgrove, Boys Town National Research Center and were purchased from Dr. Sado, Shigei Medical Research Institute) in primary antibody diluent buffer (1% BSA, 0.1% porcine gelatin, 0.01 M PBS, pH 7.2) for 1 h at room temperature. The slide were then washed twice with PBS and incubated with anti-rabbit FITC-conjugated secondary antibody (dilution 1:1000 in PBS, Jackson ImmunoResearch Laboratories) for 1 h at room temperature. The slides were mounted with Vectashield Mounting Medium with DAPI (Vector Laboratory) and glass coverslips. All slides were analyzed using the Axioskop 2 fluorescent microscope, AxioCam HRC camera, and the Axiovision 4.3 software.

Extracellular Matrix (ECM) Protein Extraction and Western Blot Analysis of Type IV Collagen Chain Expression—Mouse kidney, lung, and testes ECM proteins were prepared as previously described (27). Briefly, kidneys were homogenized in PBS with proteinase inhibitors before DNase I digestion in 1 M NaCl. The proteins were then incubated in 2% sodium deoxycholate and collagenase (CLSPA, Worthington Biochemical Corp.)-digested. Type IV collagen hexamers in the supernatant of the collagenase digest were precipitated with 95% ethanol. This technique allows for type IV collagen matrix extraction with nearly no intracellular protein contamination. Before Western blotting analyses, protein concentrations were normalized using BCA assay (Thermo Scientific, according to the manufacturer's directions). The proteins are reduced and denatured in SDS-Laemmli buffer supplemented with β-mercaptoethanol, and after SDS-PAGE and transfer onto PVDF membranes, equivalent protein loading was controlled by Coomassie staining (data not shown). Western blot analysis was performed using standard methods and using anti-mouse α1-α6NC1 antibodies (dilution 1:10,000, a gift from Dr. Cosgrove, Boys Town National Research Center and purchased from Dr. Sado, Shigei Medical Research Institute at a 1:500 dilution, as previously described (28)) as well as anti-human α5NC1 antibody (dilution 1:10,000, Wieslab AB) in 5% milk in Tris-buffered saline with Tween 20 (TBS-T). Anti-rabbit horseradish peroxidase secondary conjugated antibody was used at a 1:10,000 dilution (Sigma) also in 5% milk in TBS-T. 5% BSA in TBS-T was used to block blots when using the antibodies purchased from Dr. Sado, Shigei Medical Research Institute and diluted in 3% BSA in TBS-T.

Immunoprecipitation—100 μg of collagenase-digested ECM proteins from $A3_mA5_h$ KI and human kidneys was resuspended in 1 ml of immunoprecipitation (IP buffer: 50 mM Tris, 150 mM NaCl pH 7.5, 1% Triton-X, and proteinase inhibitors) and incubated overnight with anti-human α5 NC1 antibody. 100 μl of pre-equilibrated protein A/G PLUS-agarose beads (Santa Cruz) were then added, and samples were incubated for 4 h at 4 °C. Control samples were incubated with beads only. The beads were washed 5 times with IP buffer and boiled for 10 min in 100 μl of SDS-Laemmli buffer supplemented with β-mercaptoethanol before Western blot analyses.

Urine Albumin/Creatinine—Mouse urine samples were collected at 8, 12, and 22 weeks of age. Creatinine concentration

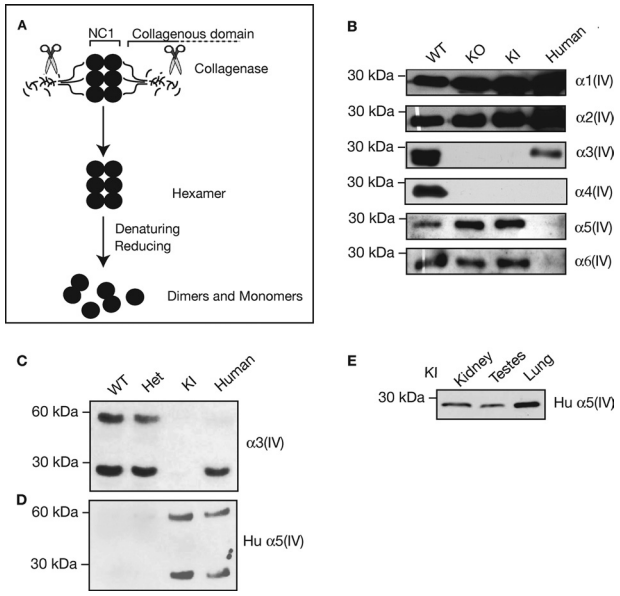

FIGURE 3. **The chimeric mouse α3/human α5 chain in the $A3_mA5_h$ KI kidney assembles into protomers associated with type IV collagen network.** *A*, shown is a schematic of ECM proteins extraction. Total kidney ECM was collagenase-digested to obtain type IV collagen NC1 hexamer, which can subsequently be denatured and reduced to monomers and dimers. *B*, shown are Western blot analyses of kidney ECM proteins extracted from human, WT, KO (ablation of mouse α3NC1 domain), and $A3_mA5_h$ KI mice for α1-α6NC1. *C* and *D*, shown are Western blot analyses of kidney ECM proteins extracted from human, WT, $A3_mA5_h$ heterozygous (*Het*) and KI mice for α3NC1 (*C*) and human α5NC1 (*D*). Monomers are detected at ~30 kDa, and dimers are at ~60 kDa. *E*, Western blot analyses of ECM proteins extracted from kidney, lung, and testes of KI mice are shown.

was measured using the colorimetric assay Quantichrome (DICT-500) from BioAssays (Hayward, CA) according to the manufacturer's directions. Albumin concentrations were measured using the Mouse Albuminuria ELISA (Bethyl Laboratories, Montgomery, TX) according to the manufacturer's directions.

Electron Microscopy—1 mm^3 of kidney sections were fixed overnight (in 2% glutaraldehyde in 0.1 M cacodylic acid, pH 7.4). Tissue specimens were post-fixed with 1% osmium tetroxide, dehydrated, and embedded in Embed 812 (Electron Microscopy Sciences, Hatfield, PA). The blocks were sectioned at 75 nm on a Leica UCT ultramicrotome (Bannockburn, IL) using a Diatome diamond knife (Electron Microscopy Sciences). Images were taken on a Technia G12 Biotwin TEM (FEI, Hillsboro, OR) equipped with an AMT CCD camera (Advanced Microscopy Techniques, Danvers, MA). All processing, sectioning, and scope work was done in the Electron Microscopy Center, Department of Anatomy and Cell Biology at the Indiana University School of Medicine.

Statistical Analyses—S.E. were calculated, and *t* test and analysis of variance were used to determine statistical differences. A level of $p < 0.05$ was considered statistically significant (*, $p < 0.05$).

Molecular Modeling—A model of the mouse α1α2α1 hexamer was created by mutating the protein chains in the crystal structure of the human placental α1α2α1NC1 hexamer (PDB ID 1LI1) (29) to the corresponding mouse sequences. Recent work identified specific interactions between the N-terminal 58 amino acids from the human α3NC1 and the α5NC1 domain.

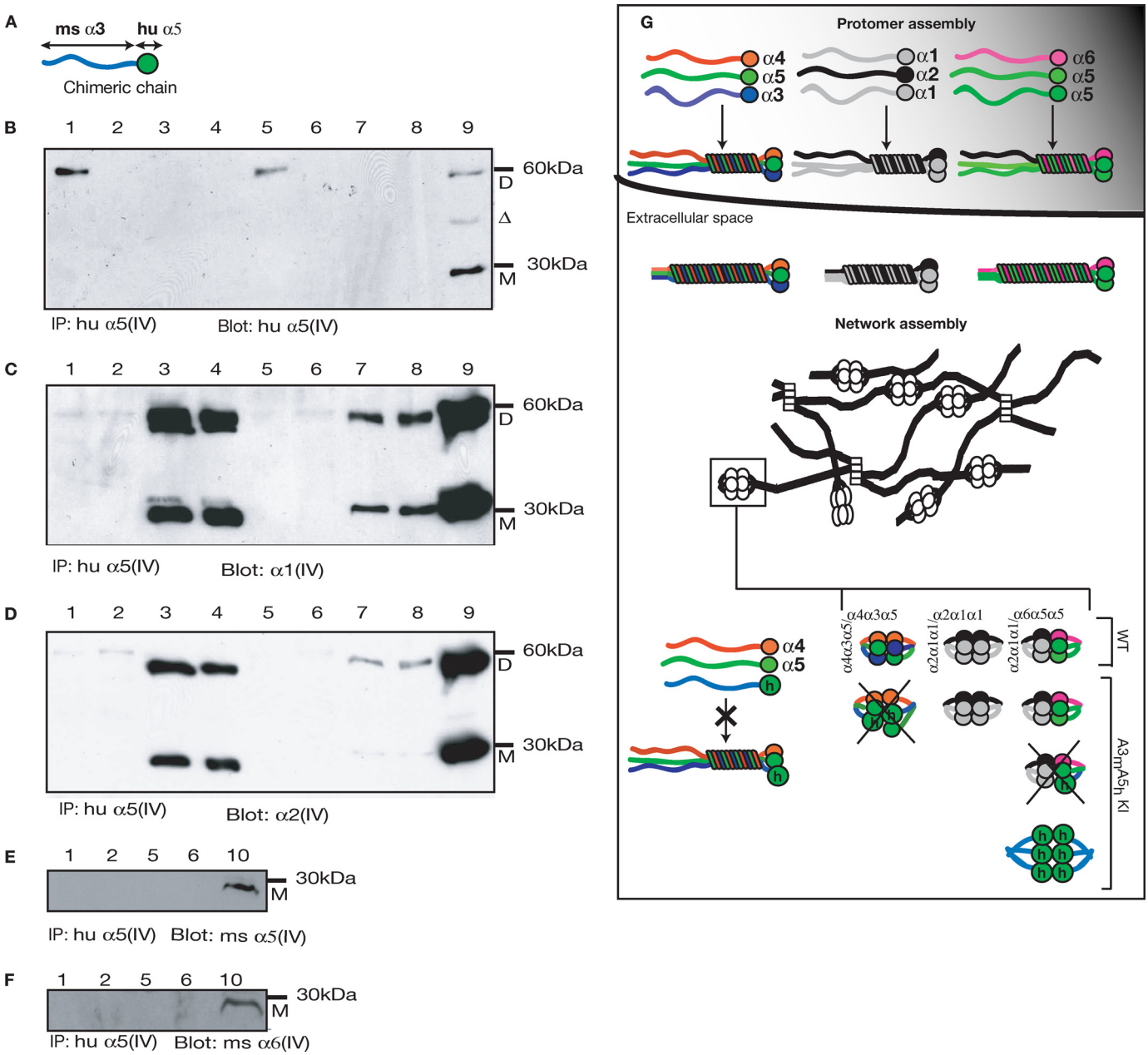

FIGURE 4. **Immunoprecipitation studies.** *A*, the chimeric mouse (*ms*) α3/human (*hu*) α5 chain (composed of the mouse α3 7S and collagenous domain and human α5NC1 domain)-containing hexamers were subjected to immunoprecipitation using a specific antibody to human α5NC1 domain. *B–F*, the bound and unbound proteins were analyzed by Western blot using antibodies anti-human α5NC1 (*B*), α1NC1 (*C*), α2NC1 (*D*), mouse α5NC1 (*E*), and mouse α6NC1 (*F*). The supernatant of the immunoprecipitation reaction (unbound) was also analyzed, and total kidney ECM from human and KI kidneys was used for positive control. The blots were loaded as follows: *1*, human kidney ECM, immunoprecipitated using anti-human α5NC1 antibody; *2*, human kidney ECM, immunoprecipitation beads only; *3*, supernatant from human kidney ECM IP using anti-human α5NC1 antibody; *4*, supernatant from human kidney ECM IP with beads only; *5*, KI kidney ECM immunoprecipitation using anti-human α5NC1 antibody; *6*, KI kidney ECM IP with beads only; *7*, supernatant from KI kidney ECM IP using anti-human α5NC1 antibody; *8*, supernatant from KI kidney ECM IP with beads only; *9*, human kidney ECM; *10*, KI kidney ECM. *D*, dimer; *M*, monomer; Δ, degradation product. *G*, schematic depiction of type IV collagen protomer assembly and type IV collagen network assembly; lack of α3NC1 domain (chimeric chain) precludes α3α4α5 protomer assembly, and the chimeric chain does not assemble into a α1α2α1/α5α6α5 network assembly but forms a unique type IV collagen network incorporating the chimeric chain, thus, highlighting a role for the 7 S and collagenous domains in network assembly.

The C-terminal region of the α5NC1 domain from amino acids 188 to 227 was also shown to interact specifically with the α3NC1 domain (20). Using this information, we generated a model of the mouse α3α4α5 protomer by mutating the human α1 chains A and D to the mouse α3 sequence and chain B and E to the mouse α5 sequence. The mouse α4, chains C and F, were generated by homology modeling using the program MODELLER (30). The three-dimensional structure of the bovine lens capsule α2NC1 domain (PDB ID 1T60) (17), which shares 74% identity with the mouse α4NC1, was used as the template. The $\alpha4\alpha5_h\alpha5$(IV) model was constructed from the mouse α3α4α5 model by mutating the sequence of the mouse α3 NC1 chains to the human α5 NC1 sequence. All side chain conformations were adjusted to minimize inter- and intramolecular clashes using the program COOT(31). The models were superimposed by secondary structure matching (32).

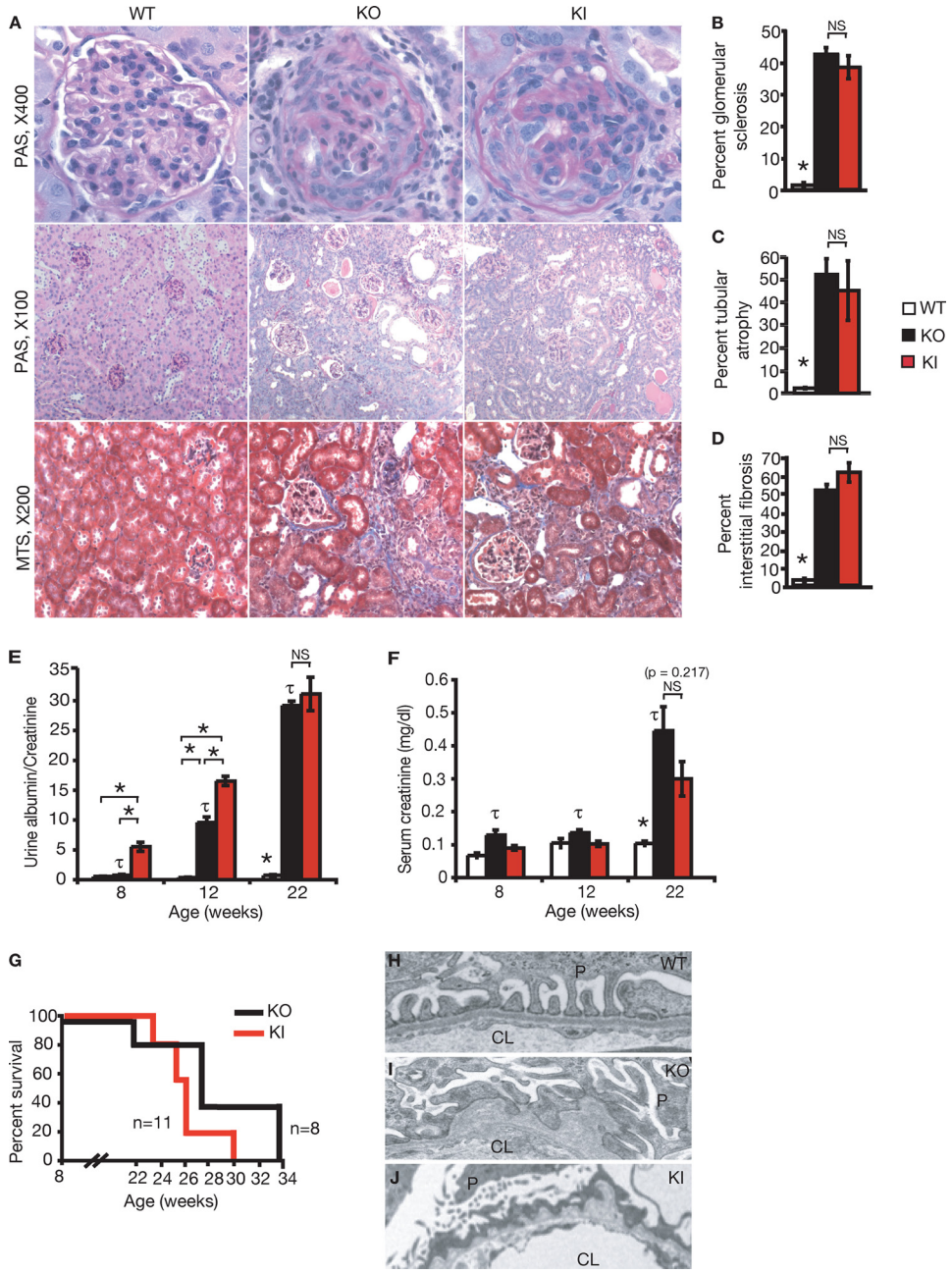

FIGURE 5. **$A3_mA5_h$ mice develop progressive glomerulonephritis associated with GBM defects.** *A–D*, shown are histological findings from periodic acid-Schiff (*PAS*) and Masson-Trichrome (*MTS*) staining of WT, KO, and KI kidneys (*A*) and morphometric analyses for glomerular sclerosis (*B*), tubular atrophy (*C*), and interstitial fibrosis (*D*). Magnification: *upper panel*, ×400; *middle panel*, ×100; *lower panel*, ×200. *NS*, not significant. *E*, shown are urine albumin/urine creatinine ratio measurements at 8, 12, and 22 weeks of age in WT (8 weeks, $n = 8$; 12 weeks, $n = 7$; 22 weeks, $n = 8$), KO (8 weeks, $n = 8$; 12 weeks, $n = 8$; 22 weeks, $n = 5$), and KI (8 weeks, $n = 6$; 12 weeks, $n = 8$; 22 weeks, $n = 6$) mice. *F*, shown are serum creatinine measurements (mg/dl) at 8, 12, and 22 weeks of age in WT (8 weeks, $n = 8$; 12 weeks, $n = 7$; 22 weeks, $n = 3$), KO (8 weeks, $n = 7$; 12 weeks, $n = 7$; 22 weeks, $n = 15$), and KI (8 weeks, $n = 8$; 12 weeks, $n = 9$; 22 weeks, $n = 6$) mice. *G*, shown are survival curve of KI mice ($n = 11$) and KO mice ($n = 8$). *H–J*, shown is an electron microscopy picture of WT (*H*), KO (*I*), and KI (*J*) GBM (*underlined*). *P*, podocyte; *CL*, capillary lumen. *, $p < 0.05$; τ, KO urine and serum samples were also used in urine albumin/creatinine and serum creatinine measurements in previous publication (26).

RESULTS

Generation of the $A3_mA5_h$ KI Mouse—We generated a DNA construct in which we substituted the genomic mouse α3NC1 domain with cDNA encoding the human α5NC1 domain (Fig. 1*A*). After screening of the embryonic stem cell clones by southern blotting and generation of F1 pups from backcrossing founder mice, we developed a genotyping protocol to ensure germ line transmission and genomic integration of the human α5NC1 sequence. WT, α3NC1 knock-out (A3KO, KO), α3NC1 knock-out/human α5NC1 knock-in heterozygous ($A3_mA5_h$ Het), and α3NC1 knock-out/human α5NC1 knock-in homozygous ($A3_mA5_h$ KI) mice tail DNA was purified and analyzed by PCR. The 350-bp DNA sequence (Fig. 1*A*) for the wild-type allele was amplified from the tail DNA of the WT and heterozygous mice but was not amplified in the homozygous KI and KO mice, confirming the specificity of the primers used to detect the wild-type allele (Fig. 1*B*). The 600-bp fragment (Fig. 1*A*) for the KI allele was amplified from the tail DNA of the heterozygous and KI mice but was not amplified in the WT and KO mice, likewise confirming the specificity of the primers used to detect the KI allele (Fig. 1*B*). The sequence identity of the 600-bp fragment was confirmed by sequencing (data not shown).

To confirm expression of human α5NC1 in the KI mice, we designed human α5NC1 specific primers that allowed for the PCR amplification of human α5NC1 from genomic tail DNA of $A3_mA5_h$ heterozygous mice (which contains the human α5NC1 cDNA sequence used in the gene construct, Fig. 1*C*). The expected 200-bp PCR product was obtained from cDNA generated from KI mouse kidney RNA but not from the cDNA generated from WT kidney RNA (Fig. 1*C*). Furthermore, human α5NC1 expression was detected using *in situ* hybridization in $A3_mA5_h$ KI mouse glomeruli but not in the WT kidney (Fig. 1, *D* and *E*). These results indicate that the integrated human α5NC1 sequence in the mouse genome is successfully transcribed in the $A3_mA5_h$ KI mouse kidney. Immunolabeling of frozen kidney tissue sections reveals a specific human α5NC1 labeling strictly in the glomeruli of KI mice (Fig. 1, *F–M*), indicating successful translation of the human α5NC1 sequence in the KI mice. Double immunolabeling against podocin, a podocyte-specific antibody, and

human α5NC1 reveal GBM labeling of the human α5NC1 (Fig. 2*A*).

Insights into Type IV Collagen Protomer Assembly in the $A3_mA5_h$ KI Mouse—Chain selection in protomer assembly is speculated to be influenced by interactions of NC1 domains between the α-chains. However, it is unclear whether the collagenous and 7 S domains play a role in chain selection. We evaluated mouse type IV collagen α-chain expression pattern in the glomeruli of WT, KO, and KI mice (Fig. 2, *B–G*). Our immunolabeling experiments revealed mesangial area labeling of mouse α1 and α2 chains in all mice, with an increase in α2 labeling in the KI glomeruli (Fig. 2, *B* and *C*), whereas in the GBM, mouse α3 and α4 chain labeling was restricted to the WT glomeruli, and α3 and α4 chain labeling in the KO and KI mice was not detected (Fig. 2, *D* and *E*). Using specific anti-mouse α5 and α6 chain antibodies (that do not cross-react with human chains; data not shown), mouse α5 and α6 chains were detected in the Bowman's capsule, and mesangium was detected in WT glomeruli and diffusely in the Bowman's capsule, GBM, and mesangium of the KO and KI glomeruli (Fig. 2*F*), with a marked increase in mesangium and GBM labeling for the α6 chain in the KO and KI glomeruli (Fig. 2*G*). Taken together, these results suggest a different pattern of α chain expression in the glomeruli of the KI mice when compared with the WT and KO mice. The KI glomeruli, in contrast with the WT and KO glomeruli, presents with an increase in mesangial α2 and α5 chains labeling and a distinct α6 GBM immunolabeling pattern.

TABLE 1
Renal phenotype

Morphometric analyses	WT	KO	KI
	%	%	%
Glomerular sclerosis	1.4 ± 0.76	42 ± 2.13	38 ± 3.6
Tubular atrophy	2.3 ± 0.29	52 ± 6.9	45 ± 13
Interstitial fibrosis	3 ± 0.9	51.8 ± 3.2	61 ± 5.31
Proteinuria			
8 weeks	0.59 ± 0.076	0.082 ± 0.06	0.82 ± 0.16
12 weeks	0.4 ± 0.07	10.36 ± 0.99	17.37 ± 0.83
22 weeks	0.8 ± 0.17	33.6 ± 3.01	31.5 ± 0.76
	mg/dl	*mg/dl*	*mg/dl*
Serum creatinine			
8 weeks	0.065 ± 0.067	0.12 ± 0.015	0.086 ± 0.006
12 weeks	0.1 ± 0.013	0.13 ± 0.0018	0.98 ± 0.0071
22 weeks	0.1 ± 0.006	0.287 ± 0.049	0.425 ± 0.0692

To identify the role of α3NC1 in chain selection in α3α4α5 protomer formation and network assembly, we examined the collagenase-digested total kidney ECM proteins from WT, KO, $A3_mA5_h$ heterozygous, KI, and human kidneys. We analyzed the extracted NC1 hexamers to reflect on secreted protomers that can assemble into type IV collagen network. The hexamers were then denatured and reduced to obtain NC1 monomers and dimers (Fig. 3*A*). The WT, KO, KI, and human kidney ECM protein samples were blotted against all six chains of type IV collagen (Fig. 3*B*). Although the antibodies against mouse α1-, α2-, and α3NC1 cross-react with human chains, the antibodies against α4, α5, and α6NC1 are specific to mouse chains and did not label human kidney ECM (Fig. 3*B*). The α1 and α2 chains were detected in all samples, whereas the kidney hexamers from KO and KI mice lacked the α3 and α4 chains. The α5 and α6 chains were detected in all mouse kidneys, corroborating our immunolabeling results (Fig. 2, *B–G*). Although the antibody against the α3 chain cross-reacts with human α3 chain (Fig. 3*C*), mouse α3NC1 was not detected in the KI kidney ECM in contrast with WT and heterozygote controls (Fig. 3*C*). The ECM protein preparations blotted with the antibody specific against the human α5NC1 domain. This antibody is highly specific to human α5NC1 and does not cross-react with any WT (Fig. 3*D*) and KO (data not shown) mouse kidney ECM proteins. Human α5NC1 dimers and monomers were only detected in the KI and human ECM protein samples (Fig. 3*D*). These results confirm that the KI mice lack the mouse α3NC1 and that the chimeric chain composed of the mouse α3 7S- and collagenous domains and the human α5NC1 domain assembles into protomers, which can be extracted from hexamers and, thus, clearly indicates assembly into the type IV collagen network in the kidney. The mouse α3/human

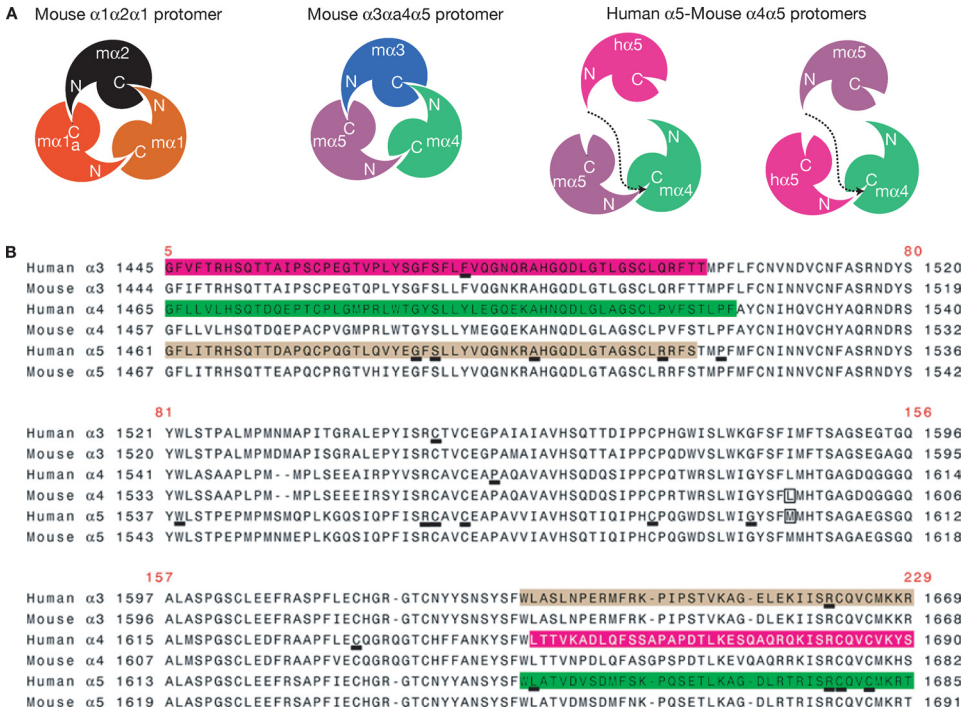

FIGURE 6. **Recognition sequences for NC1 interaction and "lock and key" NC1 domain assembly in type IV collagen chain selection.** *A*, shown is a schematic representation of the N- and C-terminal lock-and-key assembly of type IV collagen protomers. In the chimeric human α5-mouse α4-α5 schematic the *arrow* points to preferred binding site. *N*, N terminus of the NC1 domain; *C*, C terminus of the NC1 domain. *B*, shown is sequence alignment of the human and mouse α3, α4, and α5(IV) NC1 domains. The sequences were aligned using the program ClustalW (34). *Hyphens* represent gaps inserted for optimum alignment. The standard NC1 numbering scheme is shown in *red*. Missense mutations associated with Alport syndrome are *underlined*. *Highlighted sequences* represent putative coding sequence for binding between NC1 terminals.

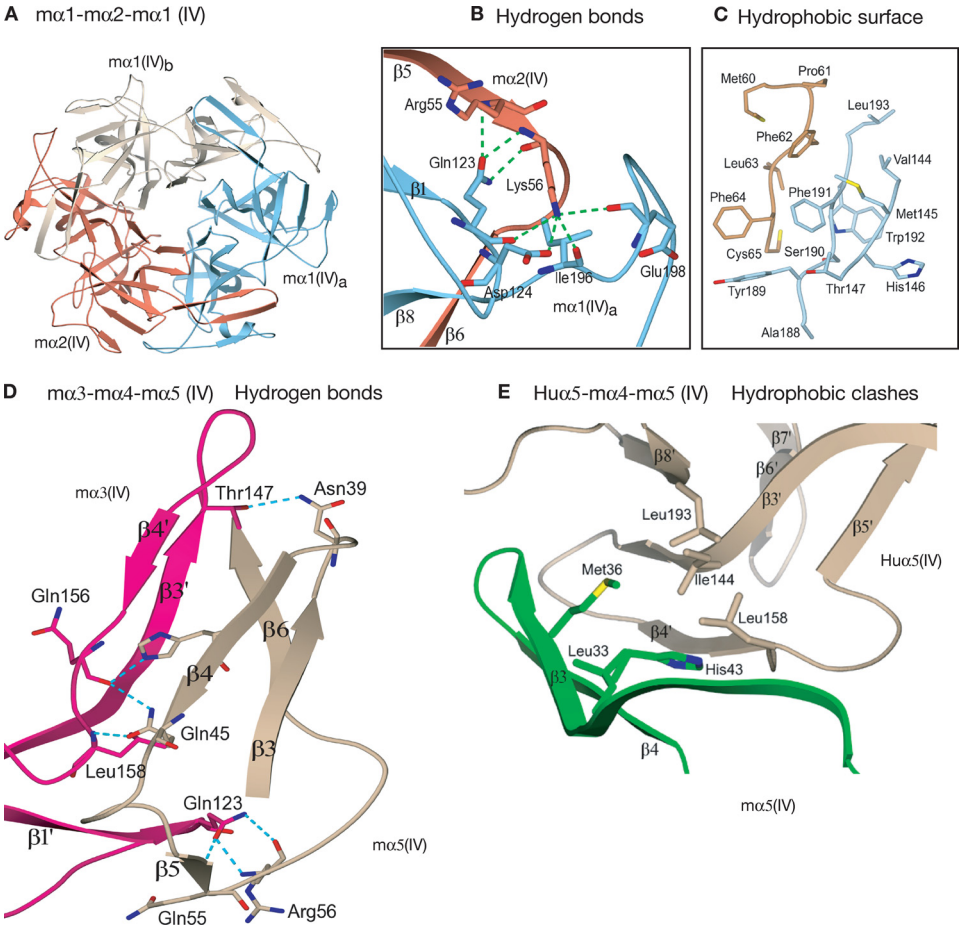

FIGURE 7. **Modeling of the type IV collagen protomer assembly.** *A–E*, shown is modeling of the mouse type IV collagen protomer. *A*, shown is a ribbon representation of the mouse $\alpha1\alpha2\alpha1$ protomer model. The positions of the secondary structure elements were calculated using the program STRIDE (35). $\alpha1_a$, $\alpha1_b$, and $\alpha2$ NC1 domain chains are colored in *brown*, *blue*, and *purple*, respectively. The secondary structure elements of $\alpha1_a$ NC1 domain are labeled. *B*, hydrogen bonds between the mouse $\alpha1_b$ and mouse $\alpha2$ NC1 domains are shown. *C*, shown are hydrophobic interactions between mouse $\alpha1_a$ and $\alpha1_b$ NC1 domains. *D*, hydrogen bonds between the mouse $\alpha3$ and mouse $\alpha5$ NC1 domains are shown. *E*, shown are hydrophobic interactions between mouse $\alpha4$ and human $\alpha5$NC1 chains in a hypothetical human $\alpha5$/mouse $\alpha4\alpha5$(IV) protomer.

$\alpha5$ chimeric chain was also detected in the lung and testes basement membrane of the KI mice (Fig. 3*D*). Importantly, mouse $\alpha4$NC1 domain was not detected in the KI ECM of the kidney, thus indicating that without the $\alpha3$NC1 domain, despite intact $\alpha3$ 7 S and collagenous domains in the KI kidneys, the $\alpha3\alpha4\alpha5$ protomer does not assemble. The $\alpha3$NC1 domain is, thus, essential for $\alpha3/\alpha4$ chain incorporation into the $\alpha3\alpha4\alpha5$ protomer.

Insights into Type IV Collagen Network Assembly—Our analyses of extracted kidney ECM indicate that the chimeric mouse $\alpha3$/human $\alpha5$ chain translates, organizes itself into protomers, and assembles into a type IV collagen network (Fig. 3, *A* and *D*). To characterize the chain composition of the networks containing the chimeric chain (Fig. 4*A*), we immunoprecipitated human $\alpha5$NC1 containing hexamers and analyzed the chain composition (Fig. 4, *B–F*). Human and KI kidney ECM were incubated with anti-human $\alpha5$NC1 antibody and protein A/G PLUS-agarose beads (Fig. 4, *B–F*, *lanes 1* and *5*) or beads only (Fig. 4, *B–F*, *lanes 2* and *6*), and supernatant from IP reactions were collected (Fig. 4, *B–D*), and compared with human kidney ECM (Fig. 4, *B–D*) or KI kidney ECM (Fig. 4, *E* and *F*). This analysis results in a highly specific pulldown of human $\alpha5$NC1 containing complexes (dimers (*D*) and monomers (*M*), Fig. 4*B*). The chimeric chain, thus, binds to neither $\alpha1$, $\alpha2$, $\alpha5$, nor $\alpha6$ chains (Fig. 4, *B–F*), indicating that the chimeric chain likely assembles into a unique type IV collagen network containing just the chimeric chain (Fig. 4*G*). Altogether these results indicate that the GBM of the KI mice is composed of $\alpha1$ and $\alpha2$ chains, assembling into the $\alpha2\alpha1\alpha1/\alpha2\alpha1\alpha1$ network, and this network lacks the hybrid mouse $\alpha3$/human $\alpha5$NC1 chain. Although other studies have demonstrated that the full-length human $\alpha5$ chain can assemble into protomers containing mouse a-chains (8, 33), the chimeric chain in the KI mice does not lend itself to $\alpha2\alpha1\alpha1/\alpha6\alpha5\alpha5$ networks. Together, our data suggest a crucial role for the $\alpha3$NC1 in the assembly of the $\alpha4\alpha3\alpha5/\alpha4\alpha5\alpha3$ network, whereas the 7 S and collagenous domains of the chimeric chain ($\alpha3$) does not favor assembly of the chimeric chain into the $\alpha2\alpha1\alpha1/\alpha6\alpha5\alpha5$ networks (Fig. 4*G*).

$A3_mA5_h$ KI Mice Present with Progressive Glomerulonephritis Similar to A3KO Mice—The $A3_mA5_h$ heterozygous mice breed normally and give birth to progeny in expected mendelian ratios. The KI mice are fertile and give birth to normal size litter. Their weight, gait, coat color, breathing rate, and activity level appear normal, and histological findings indicate that all organs studied (heart, lung, brain, eye, stomach, pancreas, liver, spleen, gastrointestinal tract, skeletal muscle, skin, and sex organs) except for the kidney appear normal. Kidneys of young mice (8 weeks old) appear normal (data not shown), with onset of glomerular sclerosis, tubular atrophy, and interstitial fibrosis with inflammatory infiltration emerging at 12 weeks of age (data not shown). At 22 weeks of age, kidneys reveal extensive glomerular sclerosis, tubular atrophy, and interstitial fibrosis (Fig. 5*A*). A3KO and $A3_mA5_h$ KI kidneys present with a similar degree of glomerular sclerosis (Fig. 5*B*, Table 1), tubular atrophy (Fig. 5*C*, Table 1), and interstitial fibrosis (Fig. 5*D*, Table 1).

Renal function tests indicate a progressive loss of renal function in the KI mice, with increased proteinuria (increased albumin/creatinine ratio) and serum creatinine levels (Fig. 5, *E* and *F*, Table 1). At 22 weeks of age, both KI and KO mice present with similar proteinuria levels (Fig. 5*E*). No statistical significant differences in serum creatinine measurements between KO and KI mice were observed at 8, 12, and 22 weeks of age, but

TABLE 2
Predicted structural changes associated with known mutations in Alport syndrome

Chain	Mutation	Structural changes
α3	F1475S	Position 1475 in all human and mouse NC1 domains is either a Tyr or a Phe. Phe-1475 inserts into a hydrophobic pocket composed of Leu-1474, Phe-1586, Tyr-1521, and Phe-1613. Mutation to a serine would introduce a hydrophilic side chain into a hydrophobic pocket and have a destabilizing effect on the buried interior of the α3 domain.
	C1548Y	Cys-1548 is conserved in all human and mouse NC1 domain and forms a disulfide bond with Cys-1493. Consequently, the C1548Y mutation would likely lead to instability in the α3 NC1 domain secondary structure.
	R1661C	Arg-1661 is an exposed amino acid. Mutation to a cysteine is not predicted to have any effect on the folding of α3 or its interaction with other chains in the protomer. It is possible, however, that mutation to a cysteine may lead to mismatched disulfide bond formation and protomer instability.
α4	C1634S	Cys-1634 is also absolutely conserved and forms a disulfide bridge with Cys-1641. The mutation C1634S would lead to instability in the α4 NC1 domain secondary structure.
	P1572L	The P1572L mutation is likely to give rise to an altered path for the α4 main chain leading to misfolding of the protein.
α5	G1486A	Steric clash with the carbonyl of Leu-1510 may also have an effect on the formation of the disulfide bond between Cys-1509 and Cys-1564.
	S1488F	Introduces a steric clash with amino acids His-1467, Ser-1468, Arg-1563, and Cys-1564 and disrupts the disulfide bond between Cys-1509 and Cys-1564.
	A1498D	Introduces a steric clash with Tyr-1491, Gln-1493, Glu-1608, and Gly-1609.
	R1511H	Undetermined significance.
	P1517T	Pro-1517 is located at the N-terminal end of β6 and servers to redirect the main chain. Mutation to a threonine would be expected to change the orientation of the backbone and disrupt the secondary structure.
	W1538R,S	Trp-1538 is in the β8 strand and stabilizes the hydrophobic interior of the α5 NC1 chain by packing against Phe-1513, Leu-1489, Leu-1510, and Ile-1561. The shorter hydrophilic side chain of serine would be insufficient to fill the void left by the tryptophan and have a destabilizing effect on the secondary structure. Mutation to arginine would introduce a hydrophilic side chain into a hydrophobic pocket and sterically clash with several hydrophobic side chains.
	R1563Q	Undetermined significance.
	C1564S	Removes a disulfide bond.
	C1567R	Removes a disulfide bond.
	C1586F,R	Removes a disulfide bond.
	W1590G	The side chain of Trp-1590 fills a hydrophobic pocket occupied by Ile-1574, Val-1572, and Lys-1683 from the α5 chain. Glycine would be insufficient to occupy this space. Trp-1590 also makes a hydrogen bond from Nϵ1 with the side chain Glu-1552 from the α3 chain, which would be lost on mutation to a glycine.
	G1596D	Undetermined significance.
	L1649R	Introduces a steric clash with Met-1600, Lsu-1614 of α5, and Leu-1510 of α3.
	R1677P	This mutation likely leads to instability of the β-sheet secondary structure due to insertion of a proline residue in a β-strand.
	C1678W	Removes a disulfide bond.
	C1681F	Removes a disulfide bond.

serum creatinine was much higher in KI and KO than the WT mice (Fig. 5*F*). The KI mice die between 23 to 30 weeks of age (Fig. 5*G*). There was no significant difference in life span between the KO and the KI mice, suggesting that at 22 weeks of age both groups of mice present with a similar renal phenotype, leading to death from loss of renal functions. Electron microscopy analyses revealed normal GBM ultrastructure in kidneys from WT mice (Fig. 5*H*), with focal thinning and thickening of the glomerular basement membrane with podocyte foot process effacement in the KO (Fig. 5*I*) and KI (Fig. 5*J*) mice at 22 weeks of age. Taken together, these results indicate that the KI mice present with GBM defect-associated progressive glomerulonephritis leading to renal failure similar to the KO mice. Both KI and KO mice present a similar phenotype despite GBM type IV collagen chain composition in the KI mice differing from the KO GBM type IV collagen chain composition, with the chimeric chain expressed and assembled into type IV collagen network in the KI mice.

Modeling the Type IV Collagen Assembly in the GBM—Our biochemical analyses from KI mice kidneys provide new insights into type IV collagen assembly, and our results provide evidence for a chain selection mechanism employing a α3NC1 domain in the organization of α3α4α5 protomers. Similarly, our results indicate that the mouse α5 chain requires mouse α3NC1 to assemble into the α3α4α5 protomer. Critical amino acids in the NC1 domain likely play a role in the chain selection leading to specific assembly of the α3α4α5 protomer (20) (Fig. 6, *A* and *B*).

We generated molecular models for the mouse α1α2α1, α3α4α5, NC1 hexamers and the hypothetical mouse $\alpha5_h\alpha4\alpha5$ protomer containing the human α5sequence NC1 substituting the mouse α3 NC1 sequence. The mouse α1α2α1 NC1 hexamer model was made using the crystal structure of the human placental α1α2α1 trimer (PDB ID 1LI1) (29), which shares 95.2% sequence identity (96.8% similarity) with the mouse α1α2α1 NC1 trimer as a template. Given the highly similar sequence identity, we simply mutated the side chains to the corresponding mouse sequences. Recent work identified specific interactions between the N-terminal 58 amino acids of the human α3 NC1 domain and α5 NC1 domain. The C-terminal region of the α5 NC1 domain from amino acids 188–227 was also shown to interact specifically with the α3 NC1 domain (20). Using this information we generated a mouse α3α4α5 model by mutation and homology modeling. The human α1 sequence shares 71.2% sequence identity (83.4% similarity) with the mouse α3 and 81.2% sequence identity (90.8% similarity) mouse α5 sequence; therefore, we mutated the human α1 chains A and D of the human placental α1α2α1 protomer x-ray structure to the mouse α3 sequence and α1 chains B and E to the mouse α5 sequence. The mouse α4 model was made by homology modeling using the program MODELLER (30) with the x-ray structure of the bovine lens capsule α2 NC1 domain, which shares 72.5% identity (82.5% similarity) as the template model (PDB ID 1T60) (17). Additionally, we analyzed the quality of the mouse α1α2α1 and α3α4α5 models using the program ProSA II. The energy profile diagrams for the mouse α1α2α1 and α3α4α5 models were plotted as a function of residue number for each chain and superimposed on the corresponding chains from the crystal structure of the human pla-

cental $\alpha1\alpha2\alpha1$ (supplemental Figs. 1 and 2). These data show that there are no major errors in the modeling.

We identify in the mouse $\alpha1\alpha2\alpha1$ protomer (Fig. 7*A*) important hydrogen bonds (Fig. 7*B*) and hydrophobic surface interactions (Fig. 7*C*) between mouse $\alpha1$ chain and mouse $\alpha2$ NC1 domains. The hydrogen bonding interactions are possible between the side chain NZ and Lys-56 in the mouse $\alpha2$ chain and the main chain of Asp-124, Gln-23, and Ile-196. The carbonyl and amides of Arg-55 and Lys-56 also make hydrogen bonds with the side chain OE1 of Gln-123 (Fig. 7*B*). Favorable hydrophobic surface interactions are also possible between the mouse $\alpha1_a$ and mouse $\alpha1_b$ chains involving the side chains of Met-60 with Cys-65 in the $\alpha2$(IV), Val-144 with Thr-147, and Ala-188 with Leu-193 (Fig. 7*C*). Based on this analysis, we identify specific amino acids interactions in that could prevent assembly of the $\alpha5_h\alpha4\alpha5$ protomer. In the mouse $\alpha3\alpha4\alpha5$ protomer model (Fig. 7*D*), it is possible for Ile-144 from the $\alpha3$ chain to insert into a shallow hydrophobic pocket composed of Leu-158 and Leu-193 from the $\alpha3$ chains and Met-36, Leu-33, and His-34 from the $\alpha4$ chain. In the hypothetical $\alpha5_h\alpha4\alpha5$ model, a serious hydrophobic clash between Met-114 of the $\alpha5_h$ chain and the side chains of Met-36 from the $\alpha4$ chain can result in a destabilizing effect possibly averting the formation of this protomer combination.

Using the information on amino acid substitution mutations reported in patients with Alport syndrome (Fig. 6*B*, Table 2), we analyzed the structural changes in the NC1 domain folding and interaction in the KI mice. Using the contact interface information in the NC1 domains of the mouse $\alpha3\alpha4\alpha5$ and mouse $\alpha1\alpha2\alpha1$ protomers, we highlight specific amino acid residues that appear critical in stabilizing bonds between NC1. Analyses of the contact interfaces in human $\alpha5$/mouse $\alpha4\alpha5$ NC1 interactions reveal hydrophobic clashes, which would in part avert assembly of this chimeric protomer.

DISCUSSION

Type IV collagen network is a major component of basement membranes, and their specific chain composition and organization into unique networks are critical in determining specific molecular properties and specialized functions (1–3, 11, 21). The mechanism underlying the self-assembly and intrinsic chain selection of type IV collagen protomer assembly is unknown and highlights its critical importance in type IV collagen-associated pathologies such as Alport syndrome.

In this study we generated and characterized of a novel mouse that enables to study the functional role of the NC1 domain in chain selection of protomers. The $A3_mA5_h$ KI mice possesses all normal α-chains of type IV collagen except for the $\alpha3$ chain, in which the mouse $\alpha3$NC1 domain is substituted with the human $\alpha5$NC1 domain. However, unlike the $\alpha3$KO mice, the KI mice express a chimeric mouse $\alpha3$/human $\alpha5$ chain that successfully assembles to form a protomer within the type IV collagen network. In agreement with previous studies demonstrating podocytes as the main source of the $\alpha3$ chain in the glomeruli (36), the chimeric chain is observed in podocytes and the GBM of the KI mice. Our NC1 domain genetic swapping approach provides a definitive evidence for NC1 domain-mediated chain selection in protomer formation. The $\alpha3$NC1 domain is required for $\alpha4$ chain selection in $\alpha3/\alpha4$ chain assembly in $\alpha3\alpha4\alpha5$ protomer and network formation. We, thus, speculate that the loss in the $\alpha4$NC1 domain (with the knock-in of the human $\alpha5$ NC1 domain, $\alpha4/\alpha5_{hu}$ chimeric chain) in the $\alpha4$ chain is expected to provide a similar phenotype as observed in the $\alpha3/\alpha5_{hu}$ chimeric chain.

In conclusion, our results provide the first *in vivo* evidence for NC1-mediated chain selection in the type IV collagen protomer assembly. The loss of $\alpha3$NC1 domain results in kidney disease with progressive glomerulonephritis leading to renal failure. This pathological finding underlines the type IV collagen assembly defect as the underlying mechanism for the GBM defect associated with Alport syndrome. Although the $A3_mA5_h$ KI and A3KO GBM type IV collagen composition differs, the similar renal phenotype observed in both models underlines the critical and unique biological properties of the $\alpha3\alpha4\alpha5$ protomer in sustaining glomerular filtration.

REFERENCES

1. Kalluri, R. (2003) *Nat. Rev. Cancer* **3,** 422–433
2. LeBleu, S., MacDonald, B., and Kalluri, R. (2007) *Exp. Biol. Med.* (*Maywood*) **232,** 1121- 1129
3. Khoshnoodi, J., Pedchenko, V., and Hudson, B. G. (2008) *Microsc. Res. Tech.* **71,** 357–370
4. Hudson, B. G., Reeders, S. T., and Tryggvason, K. (1993) *J. Biol. Chem.* **268,** 26033–26036
5. Borza, D. B., Bondar, O., Ninomiya, Y., Sado, Y., Naito, I., Todd, P., and Hudson, B. G. (2001) *J. Biol. Chem.* **276,** 28532–28540
6. Hudson, B. G., Kalluri, R., Gunwar, S., and Noelken, M. E. (1994) *Contrib. Nephrol.* **107,** 163–167
7. Ries, A., Engel, J., Lustig, A., and Kühn, K. (1995) *J. Biol. Chem.* **270,** 23790–23794
8. Söder, S., and Pöschl, E. (2004) *Biochem. Biophys. Res. Commun.* **325,** 276–280
9. Kobayashi, T., and Uchiyama, M. (2003) *Kidney Int.* **64,** 1986–1996
10. Timpl, R., Wiedemann, H., van Delden, V., Furthmayr, H., and Kühn, K. (1981) *Eur. J. Biochem.* **120,** 203–211
11. Yurchenco, P. D., and Furthmayr, H. (1984) *Biochemistry* **23,** 1839–1850
12. Kobayashi, T., Kakihara, T., and Uchiyama, M. (2008) *Biochem. Biophys. Res. Commun.* **366,** 60–65
13. Borza, D. B., Bondar, O., Todd, P., Sundaramoorthy, M., Sado, Y., Ninomiya, Y., and Hudson, B. G. (2002) *J. Biol. Chem.* **277,** 40075–40083
14. Boutaud, A., Borza, D. B., Bondar, O., Gunwar, S., Netzer, K. O., Singh, N., Ninomiya, Y., Sado, Y., Noelken, M. E., and Hudson, B. G. (2000) *J. Biol. Chem.* **275,** 30716–30724
15. Khoshnoodi, J., Sigmundsson, K., Cartailler, J. P., Bondar, O., Sundaramoorthy, M., and Hudson, B. G. (2006) *J. Biol. Chem.* **281,** 6058–6069
16. Khoshnoodi, J., Cartailler, J. P., Alvares, K., Veis, A., and Hudson, B. G. (2006) *J. Biol. Chem.* **281,** 38117–38121
17. Sundaramoorthy, M., Meiyappan, M., Todd, P., and Hudson, B. G. (2002) *J. Biol. Chem.* **277,** 31142–31153
18. Dölz, R., Engel, J., and Kühn, K. (1988) *Eur. J Biochem.* **178,** 357–366
19. Reddy, G. K., Gunwar, S., Kalluri, R., Hudson, B. G., and Noelken, M. E. (1993) *Biochim. Biophys. Acta* **1157,** 241–251
20. Kang, J. S., Colon, S., Hellmark, T., Sado, Y., Hudson, B. G., and Borza, D. B. (2008) *J. Biol. Chem.* **283,** 35070–35077
21. Paulsson, M. (1992) *Crit. Rev. Biochem. Mol. Biol.* **27,** 93–127
22. Jais, J. P., Knebelmann, B., Giatras, I., De Marchi, M., Rizzoni, G., Renieri, A., Weber, M., Gross, O., Netzer, K. O., Flinter, F., Pirson, Y., Dahan, K., Wieslander, J., Persson, U., Tryggvason, K., Martin, P., Hertz, J. M., Schröder, C., Sanak, M., Carvalho, M. F., Saus, J., Antignac, C., Smeets, H., and Gubler, M. C. (2003) *J. Am. Soc. Nephrol.* **14,** 2603–2610
23. Jais, J. P., Knebelmann, B., Giatras, I., De Marchi, M., Rizzoni, G., Renieri, A., Weber, M., Gross, O., Netzer, K. O., Flinter, F., Pirson, Y., Verellen, C., Wieslander, J., Persson, U., Tryggvason, K., Martin, P.,

Hertz, J. M., Schröder, C., Sanak, M., Krejcova, S., Carvalho, M. F., Saus, J., Antignac, C., Smeets, H., and Gubler, M. C. (2000) *J. Am. Soc. Nephrol.* **11,** 649–657
24. Longo, I., Porcedda, P., Mari, F., Giachino, D., Meloni, I., Deplano, C., Brusco, A., Bosio, M., Massella, L., Lavoratti, G., Roccatello, D., Frascá, G., Mazzucco, G., Muda, A. O., Conti, M., Fasciolo, F., Arrondel, C., Heidet, L., Renieri, A., and De Marchi, M. (2002) *Kidney Int.* **61,** 1947–1956
25. Cosgrove, D., Meehan, D. T., Grunkemeyer, J. A., Kornak, J. M., Sayers, R., Hunter, W. J., and Samuelson, G. C. (1996) *Genes Dev.* **10,** 2981–2992
26. Lebleu, V. S., Sugimoto, H., Miller, C. A., Gattone, V. H., 2nd, and Kalluri, R. (2008) *Lab. Invest.* **88,** 284–292
27. Sugimoto, H., Mundel, T. M., Sund, M., Xie, L., Cosgrove, D., and Kalluri, R. (2006) *Proc. Natl. Acad. Sci. U.S.A.* **103,** 7321–7326
28. LeBleu, V., Sugimoto, H., Mundel, T. M., Gerami-Naini, B., Finan, E., Miller, C. A., Gattone, V. H., 2nd, Lu, L., Shield, C. F., 3rd, Folkman, J., and Kalluri, R. (2009) *J. Am. Soc. Nephrol.* **20,** 2359–2370
29. Than, M. E., Henrich, S., Huber, R., Ries, A., Mann, K., Kühn, K., Timpl, R., Bourenkov, G. P., Bartunik, H. D., and Bode, W. (2002) *Proc. Natl. Acad. Sci. U.S.A.* **99,** 6607–6612
30. Sali, A., and Blundell, T. L. (1993) *J. Mol. Biol.* **234,** 779–815
31. Emsley, P., and Cowtan, K. (2004) *Acta Crystallogr. D Biol. Crystallogr.* **60,** 2126–2132
32. Krissinel, E., and Henrick, K. (2004) *Acta Crystallogr. D Biol. Crystallogr.* **60,** 2256–2268
33. Heidet, L., Borza, D. B., Jouin, M., Sich, M., Mattei, M. G., Sado, Y., Hudson, B. G., Hastie, N., Antignac, C., and Gubler, M. C. (2003) *Am. J. Pathol.* **163,** 1633–1644
34. Thompson, J. D., Higgins, D. G., and Gibson, T. J. (1994) *Nucleic Acids Res.* **22,** 4673–4680
35. Frishman, D., and Argos, P. (1995) *Proteins* **23,** 566–579
36. Abrahamson, D. R., Hudson, B. G., Stroganova, L., Borza, D. B., and St. John, P. L. (2009) *J. Am. Soc. Nephrol.* **20,** 1471–1479